

Weak Plaquette Valence Bond Order in the $S = 1/2$ Honeycomb $J_1 - J_2$ Heisenberg Model

Zhenyue Zhu,¹ David A. Huse,² and Steven R. White¹

¹*Department of Physics and Astronomy, University of California, Irvine, California 92697, USA*

²*Department of Physics, Princeton University, Princeton, New Jersey 08544, USA*

(Dated: June 25, 2018)

Using the density matrix renormalization group, we investigate the $S = 1/2$ Heisenberg model on the honeycomb lattice with first (J_1) and second (J_2) neighbor interactions. We are able to study long open cylinders with widths up to 12 lattice spacings. For J_2/J_1 near 0.3, we find an apparently paramagnetic phase, bordered by an antiferromagnetic phase for $J_2 \lesssim 0.26$ and by a valence bond crystal for $J_2 \gtrsim 0.36$. The longest correlation length that we find in this intermediate phase is for plaquette valence bond (PVB) order. This correlation length grows strongly with cylinder circumference, indicating either quantum criticality or weak PVB order.

PACS numbers: 75.10.Kt, 75.10.Jm, 73.43.Nq

Progress in finding realistic model quantum Hamiltonians with spin-liquid (SL) ground states has accelerated dramatically in the last two years, almost 40 years since Anderson first proposed a resonating valence bond state as a possible ground state of the triangular Heisenberg model [1]. One key recent advance was the discovery using the density matrix renormalization group (DMRG) of a gapped SL ground state in the spin-1/2 kagome Heisenberg antiferromagnet [2, 3]. Spin-liquid phases have been suggested for various other models, such as the half-filled honeycomb Fermi-Hubbard model [4] and the square lattice spin-1/2 Heisenberg antiferromagnet with second-neighbor (J_2) interactions [5, 6]. However, some skepticism has been expressed about the evidence for spin liquids in the latter two models [7, 8].

The main defining feature of a quantum spin liquid is the absence of any spontaneously broken symmetry, particularly either magnetic or valence bond order. Frustration, which discourages order, is a key ingredient of models potentially containing spin-liquid phases. Spin liquids arise in several analytic treatments and exactly solvable, simplified, but less realistic models [9]. A key feature distinguishing types of spin liquids is the presence or absence of a gap to all excitations. The kagome Heisenberg spin liquid is found to be gapped. To satisfy the Lieb-Schultz-Mattis theorem, gapped spin liquids for models with a net half-integer spin per unit cell must have “hidden” topological degeneracies in the thermodynamic limit, which depend on the topology of the system. The simplest possibility is a Z_2 spin liquid. Since local measurements cannot identify Z_2 or other topological orders, it is challenging to identify its presence in a numerical study. The degeneracies characteristic of a 2D gapped Z_2 spin liquid have not been accessible for the system sizes studied to date. Odd-width cylinders spontaneously dimerize in a pattern that is characteristic of a quasi-one-dimensional system [2, 5]. Another key feature of a Z_2 spin liquid is the presence of a $-\ln 2$ constant term correction to the linear growth of the entanglement

entropy with a subsystem perimeter. This term has now been measured in the nearest-neighbor kagome system [3] and also in the kagome system with next-nearest-neighbor interaction J_2 [10], where for $J_2 = 0.1$ the gaps are large and the entanglement entropy correction term can be measured particularly precisely. Thus, there is now solid evidence that the ground state of the kagome spin-1/2 antiferromagnet is a gapped Z_2 spin liquid.

In this letter, we examine the spin-1/2 Heisenberg antiferromagnet on the honeycomb lattice [see Fig. 1(a)] with Hamiltonian

$$H = J_1 \sum_{\langle i,j \rangle} S_i \cdot S_j + J_2 \sum_{\langle\langle i,j \rangle\rangle} S_i \cdot S_j . \quad (1)$$

where the sum over $\langle i, j \rangle$ runs over nearest-neighbor pairs of sites and the sum $\langle\langle i, j \rangle\rangle$ runs over next-nearest neighbors. We take $J_1 = 1$ [antiferromagnetic (AF)] and consider only $J_2 > 0$. Our work follows other studies of this and similar Heisenberg models [11–20], motivated by the Hubbard model results [21]. Most of these studies report a nonmagnetic phase near $J_2/J_1 \sim 0.2 - 0.4$, and we agree, but the results are in general disagreement on the range and nature of this phase. A variational Monte Carlo study indicated a spin liquid in the range from 0.08 to 0.3 [20]. A combination of exact diagonalization and valence bond treatment reported a plaquette valence bond [PVB, see Fig. 1(b)] crystal in the range 0.2-0.4 [11]. Exact diagonalization on small lattices [12] and the coupled-cluster method both suggest PVB order [13]. Earlier work reported that dimer correlations aren’t strong enough for PVB order [16]. Functional renormalization group work claims that this phase has weak dimer and plaquette responses [15]. Variational entangled plaquette states suggest that none of the order parameters remain nonzero [19]. Other theoretical work has focused on the possibility of a Z_2 SL on the honeycomb lattice and on phase transitions between Neel and staggered valence bond crystal (SVBC) phases [24–26].

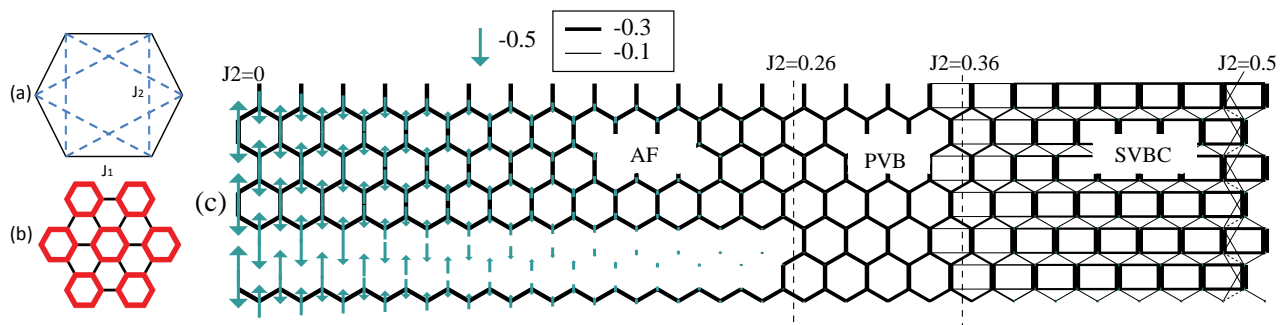


FIG. 1: (a) One hexagon of the honeycomb lattice showing J_1 and J_2 interactions. The six sides of the hexagon are J_1 bonds, and the six J_2 bonds are shown as dashed (blue) lines. (b) Illustration of the pattern of PVB order. The spin-spin correlations differ between the bonds shown as thin (black) lines versus thick (red) lines. (c) Three phases on the YC6-0 cylinder with 300 sites and a gradient of J_2 . The widths of lines are proportional to $|\langle S_i \cdot S_j \rangle|$. We also show the second-neighbor spin correlation but only when its value is negative. The arrows represent the values of $\langle S_i^z \rangle$ at each site. The scales for correlations and magnetizations are indicated. We remove several bonds in one zigzag row of the cylinder, so that the AF spin pattern is more clearly seen. The two vertical lines at $J_2 = 0.26$ and 0.36 indicate estimates of the phase boundaries.

Here, we report that the ground state displays an apparently paramagnetic phase for $0.26 \lesssim J_2 \lesssim 0.36$. For $J_2 \lesssim 0.26$, we find the usual two-sublattice AF phase. For $J_2 \gtrsim 0.36$, we find a SVBC. We have studied in some detail the system with $J_2 = 0.3$, deep within the intermediate phase that is neither AF nor SVBC. We examine various correlation functions of this ground state on various cylinders. The longest correlation length that we find is for PVB order. The strong growth of the PVB correlation length with cylinder circumference indicates that the system is either near a quantum critical point or may have weak long-range PVB order.

We use cylindrical (C) boundary conditions with open ends for our DMRG [27, 28] calculations. We label the cylinders either XCM-N or YCM-N. The labels X or Y indicated whether a first-neighbor bond is oriented horizontally (X) or vertically (Y). For XC cylinders, M is the number of sites along a zigzag vertical column and N means that the periodic boundary conditions are connected with a shift of N zigzag columns to the left or right. For YC cylinders, M is the number of zigzag horizontal rows and N means the connection has a shift by N sites along a zigzag row. For example, in the XC8-0 cylinder, one set of edges of each hexagon lies along the X direction, and there are eight sites along the zigzag columns, which are connected periodically. So, the circumference is $C = 4\sqrt{3}$ lattice spacings. For the YC4-0 cylinder, one set of edges of each hexagon lies along the Y direction and the cylinder is connected periodically along the Y direction with circumference 6 lattice spacings. For the XC9-1 cylinder, the connection has a horizontal shift of one zigzag column, producing a circumference of $C = 3\sqrt{7}$.

In Fig. 1(c), we present the ground state of a single system which gives an overview of the entire phase diagram. For this long YC6-0 cylinder, J_2 is uniform along the vertical direction, but varies linearly with the hori-

zontal position from $J_2 = 0$ at the left edge to $J_2 = 0.5$ at the right edge. To make the AF order visible, we apply a staggered field at the left end of the cylinder. As J_2 increases along the cylinder, the AF order decreases, becoming negligible in the intermediate phase. We will discuss this intermediate state in detail below. The SVBC phase appears clearly for $J_2 \gtrsim 0.36$. This SVBC phase has strong first-neighbor correlations along the vertical direction with strong horizontal second-neighbor correlations connecting them to form “ladders”. Below we will determine the phase boundaries of the AF and SVBC phases more accurately.

First, we estimate the boundary of the AF phase. One technique to determine magnetic order parameters using DMRG is to put strong ordering fields on the edges of an open cylinder, and to adjust the aspect ratio L_y/L_x to minimize the finite-size effects [29]. For both square and triangular spin-1/2 Heisenberg antiferromagnets, an aspect ratio near $1.7 \sim 1.9$ is found to minimize the finite-size effects. For XCM-0 cylinders with M columns, the aspect ratio is $\sqrt{3}$, which we use. For $J_2 = 0$, we determine that $\langle S_z \rangle \cong 0.2720$, which is close to the value determined using Monte Carlo calculations in the thermodynamic limit $\langle S_z \rangle = 0.2677(6)$ [30]. With J_2 increasing, we find that the magnetization reduces to near zero for $J_2 \cong 0.26$ in Fig. 2. The various cluster sizes all point to the phase transition near 0.26. This phase transition point is larger than the classical limit value of $J_2 = \frac{1}{6}$. Reference [20] claims that the Neel order disappears at 0.08; however, the value we find here is more consistent with other studies which give $J_2 \cong 0.2$ [11, 14].

To estimate the boundary of the SVBC phase we study several XC cylinders with J_2 varying from 0.28 to 0.40 using the method in Fig. 1. These results show the SVBC phase for $J_2 \gtrsim 0.36$. We also use the entanglement entropy and its first derivative with respect to J_2

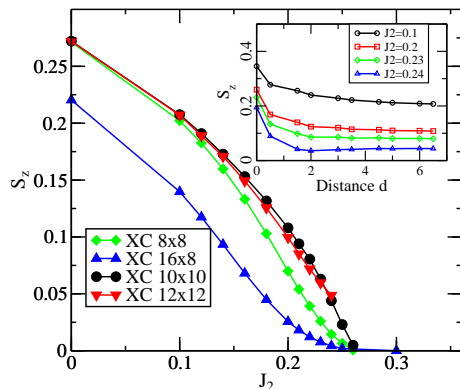


FIG. 2: The staggered magnetization at the center of the cylinder versus J_2 for various XC cylinders. The inset shows how the local magnetization decays from the edge of a long XC10 cylinder for various values of J_2 .

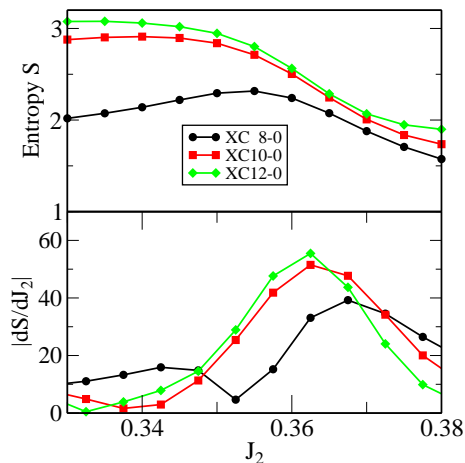


FIG. 3: The entanglement entropy and its derivative versus J_2 for different XC cylinders near the transition into the SVBC phase.

to estimate the phase transition point. We make vertical cuts between zigzag columns, the dividing line between the two parts of the system bisecting a column of horizontal bonds, and measure the entanglement entropy. As seen in Fig. 3, the entropy drops in going from the intermediate phase to the SVBC. The derivative of the entropy shows a peak around 0.37 for the XC8-0 cylinder, and around 0.36 for the wider XC10-0 and XC12-0 cylinders. In addition, the height of this peak increases with the system width, as expected for a peak indicating a phase transition [31–33].

On XC cylinders, we find that the SVBC state has strong first- and second-neighbor correlations along diagonal directions, forming diagonally oriented ladders. Thus, there are two degenerate diagonal SVBC states on an XC cylinder, whereas for YC cylinders there is only the one vertical SVBC pattern (Fig. 2). For an infinite two-dimensional system, all three of these SVBC ground

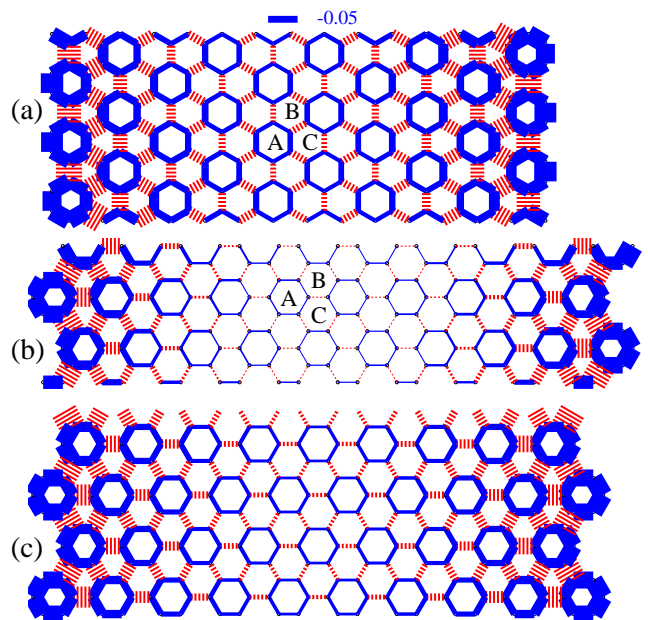


FIG. 4: Weak PVB order at $J_2 = 0.3$ on (a) YC7-3, (b) XC9-1 and (c) XC12-0 cylinders. The widths of the lines are proportional to $|\langle S_i \cdot S_j \rangle + 0.32|$ for all the plots, with solid blue(dashed red) lines for negative(positive) values. The bond strength scale is indicated at the top. The three different sublattices of plaquettes are labeled as A, B, C. In these figures, we keep $m = 6000$ states in our DMRG calculation. The truncation error for XC9-1 is smaller than 10^{-7} , while it is near 10^{-6} for the wider YC7-3 and XC12-0 cylinders.

states would be degenerate by rotational symmetry. In the classical limit, for large J_2 values, the ground state is a spin spiral state. However, quantum fluctuations are strong enough to melt the spiral order and form the SVBC, in agreement with Ref. [17].

In the rest of this letter, we focus specifically on $J_2 = 0.3$ inside the intermediate phase [34]. To measure magnetic correlations, we apply “pinning” magnetic fields at one end of the cylinder and measure the resulting magnetization pattern. Unlike in the AF phase, the induced magnetization decays exponentially from the end of the cylinder with a decay length of 2 to 3 lattice spacings for various cylinders. We further check the response to a local magnetic field applied to a spin at the cylinder center. This local magnetic field response is quite short ranged. It only influences its nearby surrounding sites, as opposed to generating a large region of staggered magnetization in the AF phase.

References [11, 12] suggest that the intermediate phase is a PVB phase with long-range dimer-dimer correlations. To investigate PVB ordering we study cylinders with periodic boundary conditions that are compatible with PVB order, including YC4-0, YC6-0, YC7-3, YC8-0, XC6-0, XC9-1 and XC12-0 [34]. We pin the PVB pattern at the cylinder ends by the choice of which spins

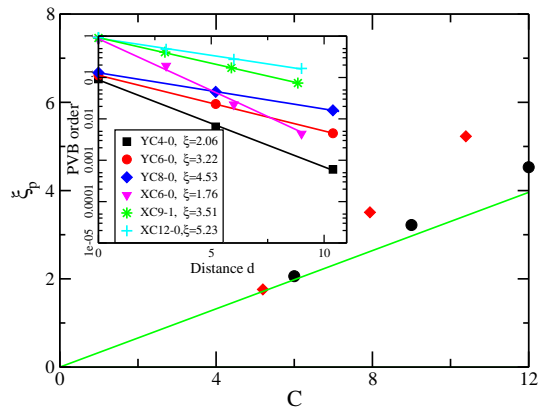


FIG. 5: PVB order correlation length ξ for different cylinder circumferences C at $J_2 = 0.3$. The black circles indicate YC cylinders, while the red diamonds indicate XC cylinders. The straight green line illustrates the expected linear behavior at the quantum critical point of the two-dimensional system. The inset shows the local PVB order parameter versus distance from the end of the cylinder in lattice spacings. The estimated PVB correlation length ξ_p is indicated for each cylinder.

are kept and how long the cylinder is (see Fig. 4).

We define a local PVB order parameter at each site using the nearest-neighbor spin correlations on the three adjacent plaquettes. The plaquettes form three sublattices in the PVB phase, as labeled in Figs. 4(a) and 4(b), and one plaquette from each sublattice is adjacent to each site. Let $E_A = -\sum_{\langle i,j \rangle} \langle S_i \cdot S_j \rangle$ be the sum over the six bonds around plaquette A. Then, we define the local PVB order parameter as

$$P = E_A + E_B \exp\left(\frac{2\pi}{3}i\right) + E_C \exp\left(\frac{4\pi}{3}i\right). \quad (2)$$

Near the ends of the cylinders, this order parameter is nonzero, and in general it is a complex number. We extrapolate this local order parameter versus the truncation error to estimate its values in the limit of large bond dimension m . For long cylinders, its magnitude decays exponentially with distance from the end, with a correlation length ξ_p that depends on the cylinder, as shown in the inset of Fig. 5. These PVB correlations can be slightly incommensurate, particularly for the narrower YC cylinders. For the XC9-1 cylinder with a shifted connection, we measure the distance from the end along the direction perpendicular to the wrapping vector to obtain the shortest PVB correlation length ξ_p .

The PVB correlation length ξ_p versus cylinder circumference C is shown in Fig. 5. This figure includes cylinders with all orientations, and we see that for our larger circumferences, the XC cylinders appear to have a longer PVB correlation length than the YC cylinders. If the 2D system is at a quantum critical point, the correlation length is expected to be proportional to the circumference by standard finite-size scaling. It appears that the

correlation length actually increases faster than the circumference, suggesting that this system may have weak PVB long-range order in the 2D limit of infinite circumference.

In conclusion, we have studied the $S = 1/2$ honeycomb $J_1 - J_2$ Heisenberg model on various cylinders extensively using DMRG. We find that the ground state displays a paramagnetic phase for $0.26 \lesssim J_2 \lesssim 0.36$. By studying PVB order on various cylinders, we find that the PVB correlation length grows at least linearly with the cylinder circumference. This suggests that in this phase the system is either quantum critical or has weak long-range PVB order. These results are compatible with an early theoretical study that a direct phase transition between an AF and a PVB state is possible on the honeycomb lattice [35].

We thank Hong-cheng Jiang, Miles Stoudenmire, Simeng Yan, Shoushu Gong, Olexei Motrunich, Donna Sheng and Tarun Grover for helpful discussion. We would also like to thank A. M. Läuchli for providing their GS energy on a small torus. This work is supported by NSF Grants No. DMR-0907500, No. DMR-1161348 and No. DMR-0819860.

Note added.—Recently we learned that Ganesh *et al.* [36] have studied the same model with DMRG. They reported that the ground state has three phases, including Neel phase, f-wave PVB state phase and dimer state phase, with critical points at $J_2/J_1 = 0.22$ and 0.35 . Their findings are generally consistent with our results, and they also make the important point that this appears to be an example of deconfined quantum criticality.

-
- [1] P. W. Anderson, Mater. Res. Bull. **8**, 153 (1973).
 - [2] S. Yan, D. A. Huse, and S. R. White, Science **332**, 1173 (2011).
 - [3] S. Depenbrock, I. P. McCulloch, and U. Schollwöck, Phys. Rev. Lett. **109**, 067201 (2012).
 - [4] Z. Y. Meng, T. C. Lang, S. Wessel, F. F. Assaad, and A. Muramatsu, Nature (London) **464**, 847 (2010).
 - [5] H. C. Jiang, H. Yao, and L. Balents, Phys. Rev. B **86**, 024424 (2012).
 - [6] L. Wang, Z.-C. Gu, X.-G. Wen, and F. Verstraete, arXiv:1112.3331 (unpublished).
 - [7] Sandro Sorella, Yuichi Otsuka, Seiji Yunoki, Sci. Rep. **2**, 992 (2012).
 - [8] A. W. Sandvik, Phys. Rev. B **85**, 134407 (2012).
 - [9] L. Balents, Nature (London) **464**, 199 (2010).
 - [10] H. C. Jiang, Z. Wang, and L. Balents, Nat. Phys. **8**, 902 (2012).
 - [11] A. F. Albuquerque, D. Schwandt, B. Hetényi, S. Capponi, M. Mambrini, and A. M. Läuchli, Phys. Rev. B **84**, 024406 (2011).
 - [12] H. Mosadeq, F. Shahbazi, and S. A. Jafari, J. Phys. Condens. Matter **23**, 226006 (2011).
 - [13] D. J. J. Farnell, R. F. Bishop, P. H. Y. Li, J. Richter and C. E. Campbell, Phys. Rev. B **84**, 012403 (2011).

- [14] J. Oitmaa and R. R. P. Singh, Phys. Rev. B **84**, 094424 (2011).
- [15] J. Reuther, D. A. Abanin, and R. Thomale, Phys. Rev. B **84**, 014417 (2011).
- [16] J. B. Fouet, P. Sindzingre, C. Lhuillier, Eur. Phys. J. B **20**, 241 (2001).
- [17] A. Mulder, R. Ganesh, L. Capriotti, and A. Paramekanti, Phys. Rev. B **81**, 214419 (2010).
- [18] D. C. Cabra, C. A. Lamas, and H. D. Rosales, Mod. Phys. Lett. B **25**, 891 (2011).
- [19] F. Mezzacapo and M. Boninsegni, Phys. Rev. B **85**, 060402 (2012).
- [20] B. K. Clark, D. A. Abanin, and S. L. Sondhi, Phys. Rev. Lett. **107**, 087204 (2011).
- [21] Note that the six spin interactions may be more important than the J_2 terms in properly characterizing the charge fluctuations in the Hubbard model [22, 23].
- [22] H.Y. Yang and K.P. Schmidt, Europhys. Lett. **94**, 17004 (2011).
- [23] H.-Y. Yang, A.F. Albuquerque, S. Capponi, A. Laeuchli, and K.P. Schmidt, New J. Phys. **14**, 115027 (2012).
- [24] F. Wang, Phys. Rev. B **82**, 024419 (2010).
- [25] Y.-M. Lu and Y. Ran, Phys. Rev. B **84**, 024420 (2011).
- [26] C. Xu and L. Balents, Phys. Rev. B **84**, 014402 (2011).
- [27] S. R. White, Phys. Rev. Lett. **69**, 2863 (1992).
- [28] S. R. White, Phys. Rev. B **48**, 10345 (1993).
- [29] S. R. White, and A. L. Chernyshev, Phys. Rev. Lett. **99**, 127004 (2007).
- [30] E. V. Castro, N. M. R. Peres, K. S. D. Beach, and A. W. Sandvik, Phys. Rev. B **73**, 054422 (2006).
- [31] A. Osterloh, L. Amico, G. Falci, and R. Fazio, Nature (London) **416**, 608 (2002).
- [32] L.-A. Wu, M. S. Sarandy, and D. A. Lidar, Phys. Rev. Lett. **93**, 250404 (2004).
- [33] O. Legeza and J. Solyom, Phys. Rev. Lett. **96**, 116401 (2006).
- [34] See Supplemental Materials for the Ground state energy per site and spin gaps (section A); cylinders that do not accommodate PVB order, such as XC8-0 and XC10-0 (section B); entropy analysis (section C).
- [35] N. Read and Subir Sachdev, Phys. Rev. B **42**, 4568 (1990).
- [36] R. Ganesh, J. van den Brink, and S. Nishimoto, arXiv:1301.0853 (unpublished).

Appendix A. Ground state energy per site and the spin gaps for $J_2 = 0.3$.

In this section, we present the ground state energies for $J_2 = 0.3$ for various cylinders in Fig. 6. The energy per site for a given cylinder is calculated by subtracting the energies of two long cylinders with different lengths [1]. We find that the energy is much lower on the narrow YC4-0 cylinder ($C = 6$), probably due to the contribution to the energy from short resonating paths that wind around the cylinder. This effect persists to a lesser extent for YC6-0 ($C = 9$). On all the other cylinders, the energy is consistently around $-0.4255(5)$ with wider cylinders having larger uncertainty due to the extrapolation to large m . Thus we estimate an approximate upper bound

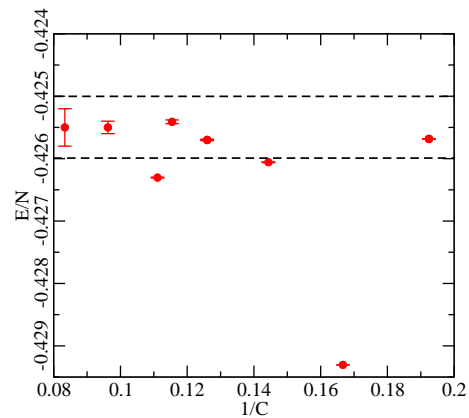


FIG. 6: The ground state energy per site at $J_2 = 0.3$ for various cylinders with circumferences C . The two dashed lines are $E/N = -0.4250$ and -0.4260 , which are the approximate upper and lower bounds of ground state energy that we estimate for the infinite two-dimensional system.

on the energy as -0.4250 . This bound is lower than other recent bounds from the variational entangled pair states method ($E \leq -0.4210$) [2, 3] and VMC ($E \leq -0.4169$) [4].

To explore the low-lying excited states on these cylinders, we apply DMRG to find the singlet and triplet gap. We lock the PVB pattern on the cylinder ends to guarantee that the excited state doesn't include translations of the PVB pattern. For the triplet gap, we target the ground state in the $S_z = 0$ and $S_z = 1$ sectors separately. We make sure the states have the expected properties, e.g. the $S_z = 0$ state has no signs of excitations and the $S_z = 1$ state has the excitation in the bulk, not at an edge. For the singlet gap, we target the ground state in the $S_z = 0$ sector first, until this state is very accurate. Then we target one more state in the same sector, with the sweeping restricted to exclude the end regions. The advantage is that the singlet excitations will always appear in the center of cylinder. We perform the calculation on long cylinders to make sure that the gap is well converged. We use length 20 for XC cylinders and length 30 for YC cylinders.

The triplet and singlet gaps for XC and YC cylinders are shown in Fig. 7. The triplet gap decreases as the cylinders get wider, with the YC cylinders having higher triplet gaps than the XC cylinders. The triplet excitations on the XC cylinders appear to consist of two well-separated spinons. This effect is more pronounced when the cylinder gets wider. In YC cylinders, it appears that the spinons remain tightly bound. We don't yet understand why the behavior is so different between the XC and YC cylinders. From the trend of the triplet gap with circumference, particularly for the YC cylinders, we estimate that in 2D limit the triplet gap is no more than 0.12. The singlet gaps also show substantial variation between different cylinders. From the trends with cir-

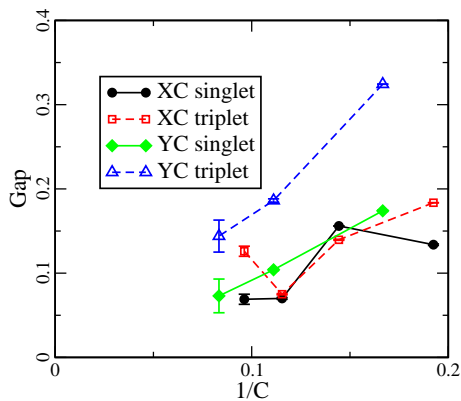


FIG. 7: (color online) Spin singlet (solid line with filled symbols) and triplet (dashed line with open symbols) gaps for various cylinders versus inverse of circumference at $J_2 = 0.3$.

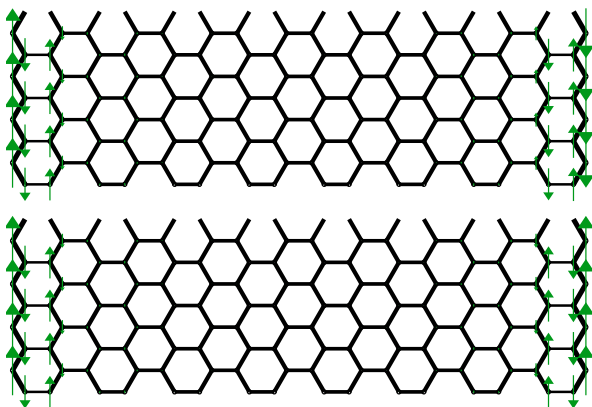


FIG. 8: Top panel shows the ground state of a XC8-0 cylinder for $J_2 = 0.3$. It has a spinon with $S_z = 1/2$ and an anti-spinon with $S_z = -1/2$ on the edges. The bottom panel shows the excited state in the $S_z = 1$ sector with two spinons on the edges. These states have almost exactly the same energy.

cumference, we estimate that in the 2D limit the singlet gap is no more than 0.07.

Appendix B. Even and odd topological sectors on XC8-0 and XC10-0 cylinders.

In this section, we will discuss the XC8-0 and XC10-0 cylinders in detail. These cylinders are not compatible with PVB order, and show interesting behavior. The frustration of the PVB order leaves two different nearly-degenerate ground states corresponding to different topological sectors. The sectors can be selected by adding or removing sites from the left and right edges. For zigzag-column left and right edges, the XC8-0 and XC10-0 ground states have two free spinons on the cylinder edges, leading to four nearly degenerate states (Fig. 8). The edge spinons can be thought of as unpaired spins in a resonating valence bond picture. Nearest-neighbor

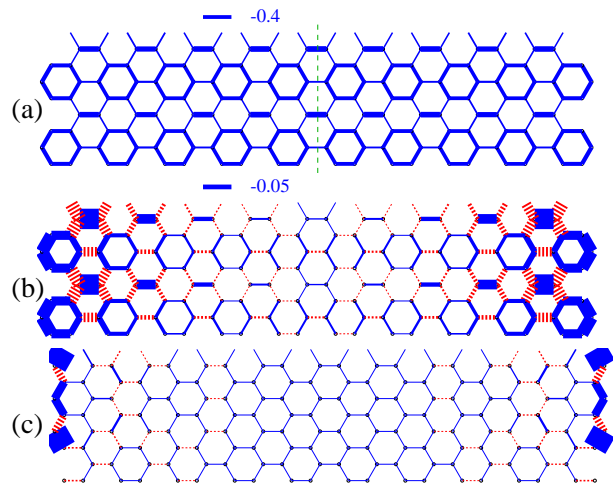


FIG. 9: (color online) (a) Initial state for the even topological sector of the XC8-0 cylinder at $J_2 = 0.3$. The width of the lines are proportional to $|\langle S_i \cdot S_j \rangle - e|$ with $e=0$. A vertical line cuts through two singlet bonds. (b) The VBC ground state for the even sector with $e=-0.32$. (c) The spin-liquid-like ground state for the odd sector with $e=-0.29$ for horizontal bonds and $e=-0.34$ for vertical bonds. The spin correlations are fairly uniform in the center. On this XC8-0 cylinder the absolute ground state is that of the odd sector.

dimer coverings of a cylinder are in two distinct topological classes, specified by whether a vertical cut through the cylinder breaks an even or odd number of dimers. We can remove one site from each end of an XC cylinder to eliminate the end spinons. Since there are then $N-1$ sites remaining on the edge of XC cylinder, this forces the dimer cover to be in the odd sector.

The opposite topological sector also can be produced by adding two vacancies inside the cylinder. The effect of vacancies is to force the the opposite topological sector between the two vacancies. The two vacancies need to sit in special locations and not too far apart; otherwise spinons may bind to the vacancies, thus keeping the system in the same sector. (not shown)

For the XC8-0 cylinder, the higher energy sector is the even topological sector, which is related to a VBC with an 8 site unit cell with a hexagon and a dimer, shown in the middle panel of Fig. 9. To get the energy per site for the even sector, we cut the ends and strengthen dimer bonds to favor the even sector initially (Fig. 9a). Then we remove these strengthened bonds to run the DMRG to get the final states (Fig. 9b). The energy splitting for the XC8-0 cylinder is shown on the left two panels of Fig. 11. The odd sector energy is always lower in the intermediate phase. This state looks more uniform (Fig. 9c) than the even sector, which shows strong valence bond order, but it has significant anisotropy. In the intermediate phase regime, the energy splitting increases with J_2 , then decreases as J_2 approaches the second phase transition point. We didn't include results from higher J_2 values,

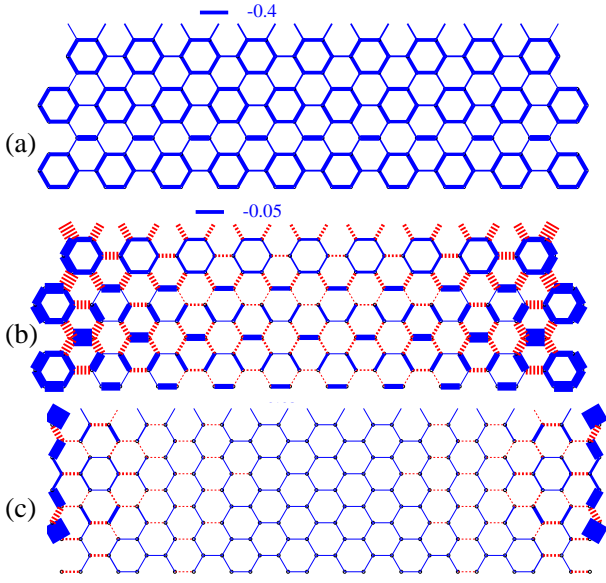


FIG. 10: (color online) Similar to previous figure, (a) and (b) are the initial and the ground state for the even topological sector of the XC10-0 cylinder with $J_2 = 0.3$. (c) is the odd topological sector. Unlike the XC8-0 cylinder, the even sector with apparent valence bond order is actually the ground state.

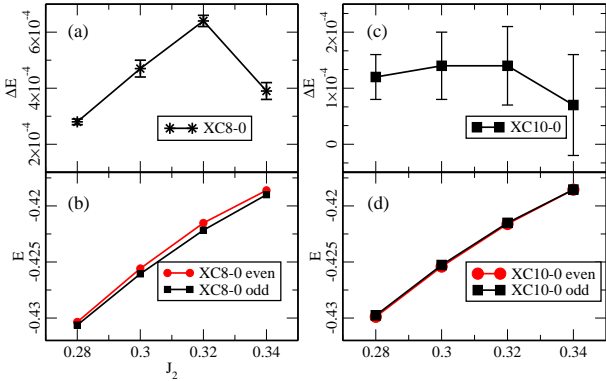


FIG. 11: (color online) Different topological sector energy splittings for the XC8-0 and XC10-0 cylinders versus J_2 with error bars. (a) and (c) are the energy splittings for the XC8-0 and XC10-0 cylinders respectively. (b) and (d) are the energy per site for both even and odd sectors on XC8-0 and XC10-0 cylinders. It's clear that on the XC8-0 cylinder the odd sector energy is lower. On the XC10-0 cylinder, the energy splitting is quite small, and becomes consistent with zero at $J_2 = 0.34$.

since the energy splitting is already small compared to the uncertainty in the extrapolation of the energy. The fact that the energy splitting reduces with J_2 as one approaches the second phase transition point means that the phase transition in to the SVBC phase happens at essentially the same J_2 value in either sector. In Fig. 3 of the main text the odd sector was used, but we also did the same analysis in the even sector, obtaining the same estimates of J_2 at the phase transition.

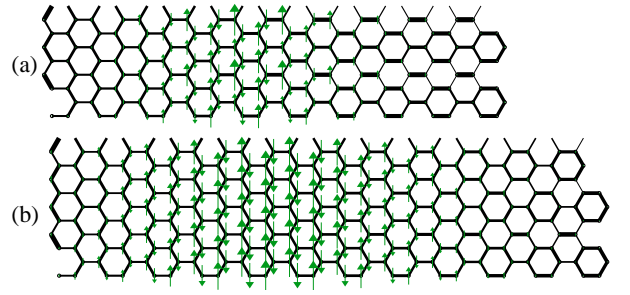


FIG. 12: (a) is XC8-0 cylinder with delta bond applied from 0.02 (left edge) to -0.05(right edge), with positive delta strengthen the vertical bonds and negative delta value strengthen the horizontal bonds. Thus we cut the cylinder edge to favor odd sector for positive delta and even sector for negative delta. Spinons locate between even and odd sectors. (b) is XC10-0 cylinder with delta from 0.01 to -0.01.

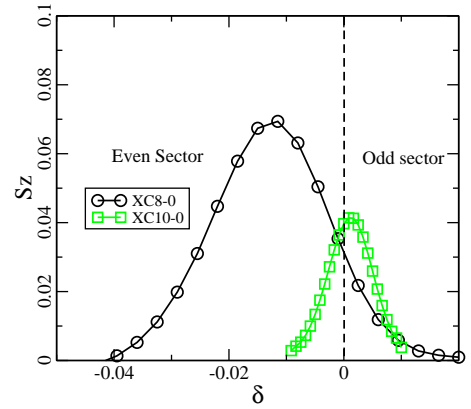


FIG. 13: Delta value versus sum of S_z along the cylinder zigzag direction for XC8-0 and XC10-0 cylinder. The data are extracted from previous figure. The left side of spinon ($\delta < 0$) is even sector, with odd sector on the spinon right side. We could see that for ground state with $\delta = 0$, XC8-0 is in odd sector and XC10-0 is in even sector.

The even sectors of XC10-0 cylinder are shown on Fig. 10. The even sector has a 20 sites VBC unit cell. The final state has stronger valence bond order than the XC8-0 cylinder. As opposed to XC8-0 cylinder, we show in the right two panels of Fig.11 that the even sector is lower in energy. We could measure the spin correlation length from placing staggered magnetic fields on the edge and measuring how S_z decays. The odd sector has a much longer spin correlation length with $\xi_s \sim 12$, as compared with roughly 3 in even sector. A longer spin correlation length usually indicate smaller spin triplet gap. We find that spin triplet gap is roughly 10^{-3} for the odd sector compared with 0.075 for the even sector. Thus these results indicate that on XC10-0 cylinder the ground state is a valence bond crystal with short range spin correlation and a nonzero spin triplet gap.

To further check that the even sector has lower energy, we strengthen and weaken some bonds to favor both sec-

tors on one cylinder; one on the left, the other on the right, see Fig. 12. A domain wall with spinon will reside between these different sectors. Depending on whether the spinon is more pushed into the even or the odd sector at $\delta = 0$, we can determine which sector is the ground state. The results are consistent on both cylinders, shown in Fig. 13.

Appendix C. Entropy analysis for intermediate phase with $J_2 = 0.3$.

In this section, we will discuss the von Neumann entanglement entropy (EE) in detail for $J_2 = 0.3$ for all the XC and YC cylinders. For a cylinder with a non-shifted connection, eg. the XCN-0 and YCN-0 cylinders, we calculate the EE for splitting the lattice into subsystems A and B. The partition is a vertical line cut through the cylinder, that always breaks the same number of horizontal or diagonal bonds, i.e. breaking $N/2$ bonds for XCN-0 cylinder and N bonds for YCN-0 cylinder. We didn't consider the EE for cylinders with shifted connections.

In a 2D disordered gapped system, the EE obeys the area law [5] with

$$S = aL + o(1/L) \quad (3)$$

where a is a non-universal constant, L is the length of the boundary between regions A and B. The second term disappears as $L \rightarrow \infty$. For a gapped topologically-ordered SL phase without broken symmetries, a extra term is included

$$S = aL + \gamma + o(1/L) \quad (4)$$

with γ is the topological EE[6, 7]. For a minimum entangled state with Z_2 topological order, $\gamma = -\ln(2)$ at $T = 0$. Thus the EE is a constant independent of length for a fixed width cylinder, since the boundary length is always the same. For a 2D critical gapless system, the EE scales as:

$$S = aL + b \ln L + c(L) \ln[\sin(\frac{\pi x}{L})] + o(1/L) \quad (5)$$

for a $L \times L$ torus[8–10]. The second term comes from gapless Goldstone mode. x is subsystem size and the third term is the function depends on ‘‘chord length’’. Thus the EE depends on system width L and subsystem size x for a 2D gapless system, but independent of subsystem size for a gapped system.

In Fig. 14(a), we show the EE versus subsystem size x for YCN-0 cylinders. Since YC cylinders have strong plaquettes appearing on the cylinder edges, we would expect that the EE should oscillate with a PVB pattern, with two high values and one low value corresponding to cuts at strong and weak bonds of plaquettes. With the

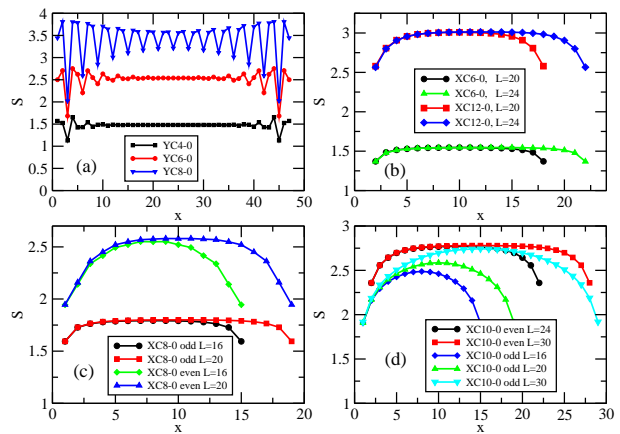


FIG. 14: (color online) The EE versus subsystem size x for (a) YC cylinders, (b) XC6-0 and XC12-0 cylinders, (c) even and odd sector in XC8-0 cylinders, (d) even and odd sector in XC10-0 cylinders. Note on YC8-0 cylinder, the EE is measured for a state with $m = 5000$. This state is not well converged and it has larger PVB order as seen in the EE oscillation pattern.

decay of PVB order to the center, we also observe the decay of the EE oscillation pattern and measure the EE when its value saturates to a constant value. We notice that YC6-0 has a longer PVB correlation length than YC4-0, since the EE oscillates with more periods near the YC6-0 cylinder edges. On the YC8-0 cylinder, the state in which we measure the EE is not well converged, and thus it has stronger PVB order. The EE shows an apparent PVB order oscillation pattern.

For the XC cylinders in Fig. 14(b-d), the entropy is saturated in the center, independent of subsystem size for the ground state. For the XC8-0 cylinder, the odd sector EE is independent of the sub-system size x and has the same value for cylinders of different lengths. The EE has much stronger dependence on the sub-system size for the even sector. On the contrary for the XC10-0 cylinder, the EE saturates in the center of the cylinder for the even sector. All these results again show that the GS for all the cylinders with $J_2 = 0.3$ are gapped with short spin correlation lengths.

In Fig. 15, we present the EE versus cylinder width to extrapolate the topological EE γ . It is surprising that not all the data points collapse onto a line. The EE from XC6-0 and XC10-0 deviates from a linear extrapolation. It is possible that XC6-0 cylinder is too narrow, so that $J_2 = 0.3$ is too close to the second phase transition point. The XC10-0 cylinder is a valence bond crystal with 20 sites unit cell in the even sector. We find that $\gamma = -0.619$, which is close to gapped Z_2 SL with $\gamma = \ln 2 = -0.693$.

In a recent paper by Hong-Chen Jiang et al.[11], the authors extrapolate the EE to get the TEE with $\gamma \sim -\ln 2$ and identify Z_2 SL phase on many models. As those au-

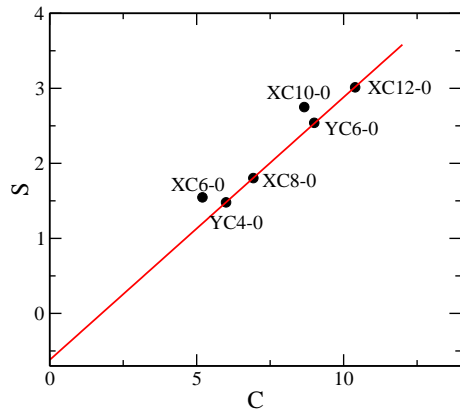


FIG. 15: Saturated EE versus cylinder circumference C for the XC and YC cylinders.

thors realize, for the above method to be accurate when identifying topological phases, all the correlation lengths (spin-spin, dimer-dimer, etc.) have to be short compared with the cylinder widths, so that DMRG results will always lead to a minimum entangled state (MES) with zero vison flux through the cylinder. For the model in this paper, even though the spin-spin correlation length is short, PVB correlation lengths get longer as the cylinder gets wider. Thus the extrapolation method for the TEE would lead to strong finite size effects. Therefore

the non-zero γ we find in this paper doesn't indicate that the GS for the Heisenberg $J_1 - J_2$ model on the honeycomb lattice is a Z_2 SL in the 2D limit.

-
- [1] E.M. Stoudenmire and S. R. White, *Annual Rev. of Cond. Matt. Phys.* **3**,111 (2012).
 - [2] F. Mezzacapo and M. Boninsegni, *Phys. Rev. B* **85**, 060402 (2012).
 - [3] We use table I of Ref. [19] at $J_2 = 0.3$. We extract the data from $L=9, 16, 18$ and extrapolate versus $L^{-3/2}$ to get the energy in the 2D limit as $L \rightarrow \infty$.
 - [4] B. K. Clark, D. A. Abanin, and S. L. Sondhi, *Phys. Rev. Lett.* **332**, 1173 (2011).
 - [5] J. Eisert, M. Cramer, and M. B. Plenio, *Rev. Mod. Phys.* **82**, 277 (2010).
 - [6] A. Kitaev, and J. Preskill, *Phys. Rev. Lett.* **96**, 110404 (2006).
 - [7] M. Levin, and X. G. Wen, *Phys. Rev. Lett.* **96**, 110405 (2006).
 - [8] M. A. Metlitski, and T. Grover, arXiv:1112.5166 (unpublished).
 - [9] A. B. Kallin, M. B. Hastings, R. G. Melko, and R. R. P. Singh, *Phys. Rev. B* **84**, 165134 (2011).
 - [10] H. Ju, A. B. Kallin, P. Fendley, M. B. Hastings and R. G. Melko, *Phys. Rev. B* **85**, 165121 (2012).
 - [11] H. C. Jiang, Z. Wang, and L. Balents, *Nature Physics* **8**, 902 (2012).